THE JOURNAL OF BIOLOGICAL CHEMISTRY VOL. 288, NO. 48, pp. 34627–34637, November 29, 2013
© 2013 by The American Society for Biochemistry and Molecular Biology, Inc. Published in the U.S.A.

# Deficiency of a Glycogen Synthase-associated Protein, Epm2aip1, Causes Decreased Glycogen Synthesis and Hepatic Insulin Resistance*[S]

Received for publication, May 6, 2013, and in revised form, October 7, 2013 Published, JBC Papers in Press, October 18, 2013, DOI 10.1074/jbc.M113.483198

**Julie Turnbull[‡§1], Erica Tiberia[‡], Sandra Pereira[¶], Xiaochu Zhao[‡], Nela Pencea[‡‖], Anne L. Wheeler[**], Wen Qin Yu[¶], Alexander Ivovic[¶], Taline Naranian[‡], Nyrie Israelian[‡], Arman Draginov[‡], Mark Piliguian[‡], Paul W. Frankland[**], Peixiang Wang[‡], Cameron A. Ackerley[‖], Adria Giacca[¶], and Berge A. Minassian[‡ ‡‡2]**

*From the [‡]Program in Genetics and Genome Biology, [‖]Department of Pathology and Laboratory Medicine, [**]Program in Neurosciences and Mental Health, and [‡‡]Department of Paediatrics, The Hospital for Sick Children, Toronto, Ontario M5G 1X8, Canada and the [§]Department of Molecular Genetics and [¶]Department of Medicine and Physiology, University of Toronto, Toronto, Ontario M5S 1A1, Canada*

**Background:** Impaired activation of glycogen synthesis is a major component of insulin resistance.
**Results:** We identified a protein, Epm2aip1, that associates with glycogen synthase (GS) and whose absence impairs allosteric activation of GS and causes hepatic insulin resistance.
**Conclusion:** Epm2aip1 is a modulator of GS activity under insulin control.
**Significance:** This study uncovers a novel component of glycogen regulation and hepatic insulin resistance.

**Glycogen synthesis is a major component of the insulin response, and defective glycogen synthesis is a major portion of insulin resistance. Insulin regulates glycogen synthase (GS) through incompletely defined pathways that activate the enzyme through dephosphorylation and, more potently, allosteric activation. We identify Epm2aip1 as a GS-associated protein. We show that the absence of Epm2aip1 in mice impairs allosteric activation of GS by glucose 6-phosphate, decreases hepatic glycogen synthesis, increases liver fat, causes hepatic insulin resistance, and protects against age-related obesity. Our work identifies a novel GS-associated GS activity-modulating component of insulin resistance.**

Under physiological conditions, the entirety of carbohydrate from a meal is rapidly absorbed and, except for what is directly consumed, is immediately packaged into glycogen (1). Glycogen synthase (GS)[3], encoded by the *GYS2* gene in liver and the *GYS1* gene in muscle and other tissues, is the rate-limiting enzyme of glycogen synthesis. GS is activated allosterically by glucose 6-phosphate (G6P), the main intracellular form of glucose, and much less potently by dephosphorylation (2). Activation of GS is a principal function of insulin, and in insulin-resistant states, a major portion of the resistance stems from the impaired ability of insulin to activate GS (3–5). Insulin activates GS through both the allosteric and dephosphorylation routes, the former through raising the levels of G6P. In skeletal muscle, insulin raises intracellular G6P mainly by translocating GLUT4 to the sarcolemma to increase glucose import and conversion to G6P. In liver, glucose transport is not regulated by insulin and is unrestricted, equivalent to free diffusion (6, 7). In that organ, insulin raises intracellular G6P transcriptionally, including by increasing expression of glucokinase and decreasing expression of glucose 6-phosphatase (6). Insulin activation of GS via dephosphorylation proceeds through inhibition of glycogen synthase kinase 3 (GSK3) (insulin receptor → Irs1/2 → PI3K → Akt ⊣ GSK3) and other GS kinases (8, 9), and promotion of GS dephosphorylation by targeting protein phosphatase 1 (PP1) to GS (10) through adaptor proteins (PTG, $G_L$, $G_M$, $R_{GL}$, or R6) that bind GS and PP1 (11).

Although GS determines the amount of glycogen, glycogen branching enzyme confers glycogen its unique spherical structure. Every six glucose units added by GS to a glycogen strand are detached by the branching enzyme as a hexamer and reattached upstream to the side of the strand through an $\alpha 1-6$ linkage. Repetitions of GS and branching enzyme actions expand the molecule radially into a dense soluble sphere containing up to 55,000 glucosyl residues. Branching enzyme deficiency (type IV glycogenosis) results in malformed glycogen molecules (polyglucosans) that resemble plant starch, with long strands and poor branching, and that, like starch, are insoluble, and precipitate and aggregate into large cytoplasmic masses that lead to hepatic cirrhosis and/or cardiac, skeletal muscle, and neurological disease (2, 12). Polyglucosans also form in a second disease, Lafora disease, in which the liver, muscle, heart, and brain exhibit increased amounts of glycogen along with the polyglucosan masses (13, 14). In the brain, polyglucosans overtake neuronal dendritic cytoplasms and provoke intractable neurodegeneration, epilepsy, and death because of massive convulsions (13). Lafora disease is caused by mutations in the

* This work was supported in part by the Canadian Institutes of Health Research.
[S] This article contains supplemental Figs. S1–S4, Methods, Data, and References.
[1] Supported by a Canada Graduate Scholarship from the National Sciences and Engineering Research Council.
[2] Holder of the Michael Bahen Chair in Epilepsy Research, University of Toronto. To whom correspondence should be addressed. Tel.: 416-813-7721; E-mail: berge.minassian@sickkids.ca.
[3] The abbreviations used are: GS, glycogen synthase; G6P, glucose 6-phosphate; LGSKO, liver glycogen synthase knock-out; MGSKO, muscle glycogen synthase knock-out.

Downloaded from http://www.jbc.org/ by guest on January 1, 2016

*EPM2A* gene, encoding a glycogen binding phosphatase (laforin), or the *EPM2B* gene that encodes an E3 ubiquitin ligase (malin) that interacts with laforin (13, 15). The pathogenesis of Lafora disease remains unsettled. The results to date support two main hypotheses. 1) The laforin-malin complex regulates PTG and GS, and the absence of laforin or malin leads to increased GS activity, excessive elongation of glycogen strands, and conversion of GS to polyglucosan (16, 17). 2) The laforin-malin complex regulates glycogen phosphorylation, its deficiencies resulting in glycogen hyperphosphorylation and consequent precipitation and gradual conversion to polyglucosan (14, 18).

Here, we characterize Epm2a-interacting protein 1 (Epm2aip1), a laforin-interacting protein (19) of unknown function. We find that Epm2aip1 associates with GS and that its absence results in reduced allosteric activation of GS by G6P and in hepatic insulin resistance.

## EXPERIMENTAL PROCEDURES

*Generation of Epm2aip1$^{-/-}$ Mice*—The *Epm2aip1* gene-trapped embryonic stem cell line (BA0314) was obtained from the Sanger Institute Gene Trap Resource (SIGTR) (Fig. 1*A*). ES cells were injected into C57/BL6 blastocysts. Chimeras were bred to C57/BL6 mice and screened for positive transmission. Heterozygous mice were interbred to produce *Epm2aip1*$^{-/-}$ progeny (KO mice). Except where indicated, mice were 4–6 months old in all experiments. All glycogen metabolic studies were performed at 6 h refeeding following a 24-hour fast, except where noted. Animal procedures were approved by The Hospital for Sick Children and The Toronto Centre for Phenogenomics Animal Care Committees.

*Microscopy, Western Blotting, and Immunoprecipitation*—Standard electron and light microscopic methods were used as described previously (20). For immunofluorescence, 3T3-L1 cells were grown on glass coverslips to confluence and fixed briefly in phosphate-buffered 4% paraformaldehyde followed by permeabilization with 0.1% Triton X-100. Cells were then washed thoroughly in PBS and blocked in 0.5% BSA prior to incubation with the Epm2aip1 antibody for 1 h. Cells were then incubated with goat anti-mouse IgG antibody conjugated to Cy3 (Jackson ImmunoResearch Laboratories). Nuclei were stained with DAPI (Sigma), coverslips were mounted on glass slides in *n*-propyl gallate (Sigma). Images were acquired on a Quorum spinning disk microscope (Zeiss Axiovert 200) using a 63× water objective (Zeiss) with a numerical aperture of 1.2 equipped with a Hamamatsu C9100-13 electron multiplying charge-coupled device camera. Images were collected and processed with Volocity 4.4.1. (Improvision Ltd.)

Monoclonal Epm2aip1 antibody was from Abnova, and GS and p641GS antibodies were from Cell Signaling Technology. Lysates for Western blot analyses were prepared from tissues using homogenization buffer and protease/phosphatase inhibitors (Roche). To assess the amount of glycogen-bound GS, lysates were centrifuged at 200,000 × *g* to obtain the glycogen pellet after an initial 1,500 × *g* centrifugation to remove cellular debris. Protein ratios in each fraction were calculated by normalizing to GAPDH levels using TotalLab Quant.

Immunoprecipitation was performed as described previously (20) using an HA-tagged Epm2aip1 construct (19) and a Myc-tagged GS construct containing the full-length coding sequence of Gys1 in pcDNA3.1 (Invitrogen).

*Biochemical Assays*—Glycogen levels were measured as described previously (18). Glycogen synthase activity was measured in the presence of varying concentrations of its allosteric activator, G6P, as listed for each experiment. Protein samples were added to a reaction mixture containing 50 mM Tris-HCl (pH 8.0), 20 mM EDTA, 25 mM potassium fluoride, 10 mg/ml glycogen, 7.2 mM UDP-glucose, 0.5 μCi/ml UDP-[$^{14}$C]glucose, and the stated concentration of G6P. Reactions were incubated at 37°C for 10–30 min and purified on G50 columns (21). The amount of radiolabeled glucose incorporation into glycogen was calculated using a scintillation counter. Fractional activity was calculated as the ratio between low G6P and high G6P. For GS assays using skeletal muscle after exhaustive exercise, mice were trained for 4 days (3 min/day) on a treadmill. On the first training day, the treadmill incline was set to 5°, and the speed was set at 8 m/min. Speed was increased by 1 m/min during the training session to 10 m/min. For each following training day, the incline was increased by 5°, and the initial speed was increased by 1 m/min. Following training, mice were fasted for 16 h and then placed on the treadmill to run at 12 m/min at an incline of 20° for 2.5 h or until exhaustion, as judged by refusal to remain on the treadmill. A mild electrical stimulus (16–28 V) was applied to mice that stepped off the treadmill belt occasionally, or a plastic straw was used to brush the mice.

*Insulin and Glucose Tolerance Tests*—For insulin tolerance tests, mice were fasted for 4 h before receiving intraperitoneal injection of insulin at time 0. Male mice were given 0.75 milliunit/g body weight insulin and female mice 0.5 milliunit/g body weight insulin (Humulin, Eli Lilly). Blood glucose levels were measured at 0, 15, 30, 60, and 120 min (Abbott). For glucose tolerance tests, mice were fasted overnight (14–16 h). Glucose was injected intraperitoneally at 2 mg/g body weight (18, 22), and blood glucose levels were measured at 0, 15, 30, 60, and 120 min. Areas under or above the curve were calculated as described previously (23).

*Hyperinsulinemic-Euglycemic Clamps*—Hyperinsulinemic-euglycemic clamps were performed as described previously described (24). Mice fasted for 3 h were given a primed infusion of [3-$^{3}$H] glucose at −120 min, and basal glucose production was measured from −30 to 0 min. At time 0, a continuous infusion of insulin (3 milliunits/kg/min) was started, and plasma glucose was maintained constant via a variable glucose infusion adjusted according to plasma glucose levels obtained every 10 min. The glucose infusion was radiolabeled to minimize changes in plasma glucose-specific activity. Endogenous glucose production and utilization were determined in the last 30 min of the 120-min clamp.

*Statistical Analysis*—Data are shown as mean ± S.E. Significance was evaluated using an unpaired Student's *t* test, and values were considered significant at $p < 0.05$ unless stated otherwise stated.

Downloaded from http://www.jbc.org/ by guest on January 1, 2016

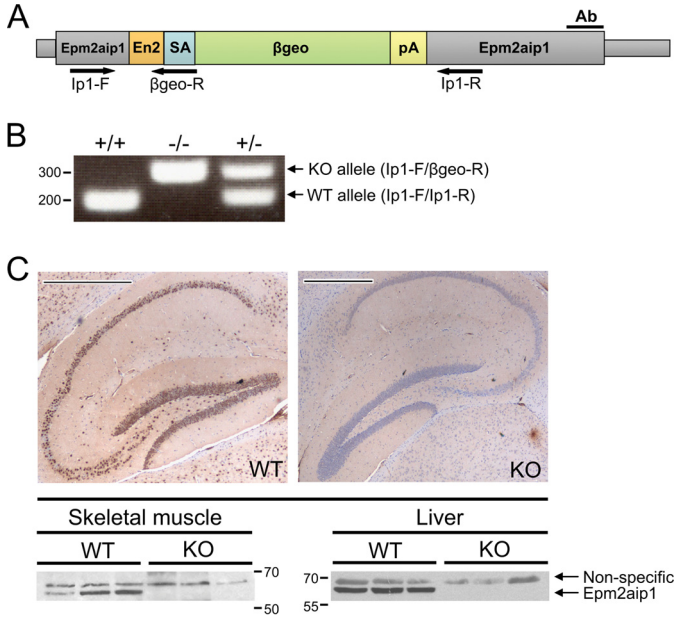


FIGURE 1. **Generation and characterization of the *Epm2aip1*$^{-/-}$ null mouse line.** *A*, schematic of the *Epm2aip1* gene trap allele. The En2-SA-βgeo-pA trap (*En2*, 1.5 kb of the *En2* gene; SA, splice acceptor site; pA, poly(A) tail; *βgeo*, β-galactosidase-neomycin resistance fusion) inserts near the start of the single *Epm2aip1* exon. *Ab*, epitope region of the Epm2aip1 antibody used throughout this study; *IP1-F*, *IP1-R*, and *βgeo-R*, locations of PCR primers used in experiment in *B*. *B*, confirmation of *Epm2aip1* gene disruption. *C*, immunohistochemical (brain, hippocampal region) and Western blot confirmation of Epm2aip1 absence. Three different mice per genotype are shown in the Western blots. *Scale bars* = 500 μm.

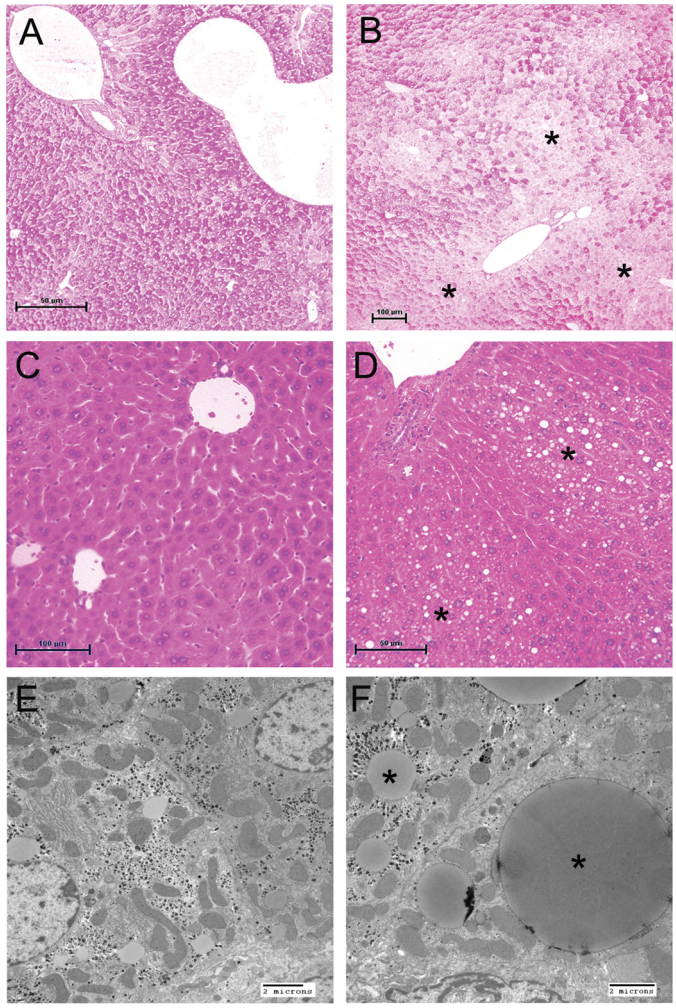


FIGURE 2. **Decreased glycogen and increased lipid in livers of *Epm2aip1*$^{-/-}$ mice.** *A*, periodic acid-Schiff staining of wild-type liver. Note the relatively homogenous staining of the acid mucosubstances (glycogen) in the majority of the liver parenchymal cells. *B*, periodic acid-Schiff staining of *Epm2aip1*$^{-/-}$ mouse liver. Large areas of the liver parenchyma have little or no staining (*asterisks*). These areas are predominantly in zone 1 (periportal) of the liver lobule (note the portal triad in the center of the main glycogen-poor region), which is the zone that is repleted last and depleted first during normal cycles of liver glycogen formation-consumption (29). *C*, hematoxylin and eosin staining of WT liver at 2 months of age. *D*, a similar area in *Epm2aip1*$^{-/-}$ mouse liver at the same age as above. Note the focal patches of steatosis (lipid accumulation) (*asterisks*). *E*, electron micrograph of WT liver. *F*, a similar area from an *Epm2aip1*$^{-/-}$ mouse liver. Note the numerous lipid droplets (*asterisks*) throughout the cell.

## RESULTS

*Epm2aip1*$^{-/-}$ *Mice Exhibit Hepatic Glycogen Deficiency*—To probe for Epm2aip1 functions, we generated mice lacking Epm2aip1 using a gene-trapped embryonic stem cell line. The trap (βgeo vector) had inserted into the extreme 5′ end of the single exon of *Epm2aip1*, disrupting the gene (Fig. 1*A*). *Epm2aip1*$^{-/-}$ pups are born at expected Mendelian frequencies and are fertile. DNA analysis by PCR confirms the insertion and the absence of a WT *Epm2aip1* sequence (Fig. 1*B*). Immunohistochemistry and Western blotting show a complete lack of the protein (Fig. 1*C*), indicating a null allele.

*Epm2a*$^{-/-}$ and *Epm2b*$^{-/-}$ mice replicate human Lafora disease, exhibiting increased glycogen, profuse polyglucosan accumulations in the brain and other tissues, epilepsy, ataxia, motor deficits, and anxiety (18, 25, 26). We tested whether *Epm2aip1*$^{-/-}$ mice also have symptoms of Lafora disease. The mice did exhibit heightened anxiety on the basis of responses in the open field and startle tests but none of the cardinal symptoms of the disease (epilepsy, motor deficits, or ataxia). They, in fact, outperformed WT animals on the rotarod (supplemental Figs. S1–S3). Pathologically, periodic acid-Schiff staining, the standard histochemical stain for glycogen and polyglucosan bodies, showed no increase in glycogen and no polyglucosan bodies in any tissues, even at 12 months of age (supplemental Fig. S4). Collectively, these results indicated that *Epm2aip1*$^{-/-}$ mice do not have Lafora disease. Rather than increased, liver glycogen content was actually decreased (Figs. 2, *A* and *B*). Fat content was also abnormal in *Epm2aip1*$^{-/-}$ livers, in this case increased (Figs. 2, *C*–*F*). Skeletal muscle, the other major glycogen storing organ, had normal glycogen content and no lipid accumulation.

*Epm2aip1*$^{-/-}$ *Mice Have Reduced Glycogen Synthesis in Liver*—To investigate the reduced liver glycogen, we asked whether it was due, at least in part, to reduced glycogen synthesis. We fasted *Epm2aip1*$^{-/-}$ and WT mice for 24 h, which depletes liver glycogen, and then refed them for 6 h, which normally fully replenishes the glycogen (27). In WT mice, liver glycogen fully replenished, whereas in *Epm2aip1*$^{-/-}$ mice it did not. *Epm2aip1*$^{-/-}$ livers resynthesized less than half the quantity of glycogen generated by WT animals (Fig. 3*A*), confirming the presence of reduced glycogen synthesis in *Epm2aip1*$^{-/-}$ livers.

Downloaded from http://www.jbc.org/ by guest on January 1, 2016

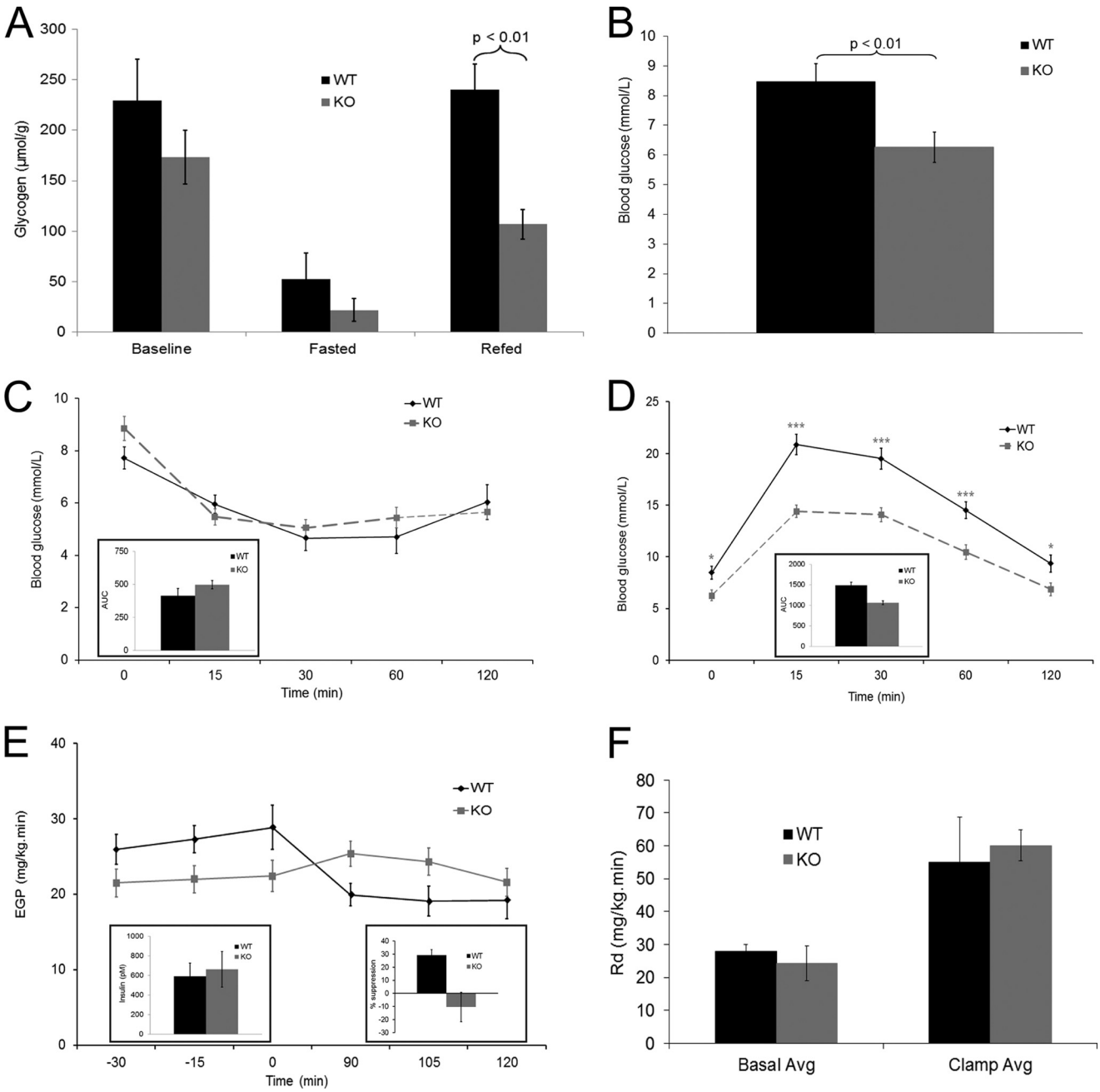


FIGURE 3. **Reduced hepatic glycogen synthesis, increased blood glucose clearance, hepatic insulin resistance, and other metabolic results.** *A*, liver glycogen levels at base line, 24 h fasted, and after 6 h of refeeding (μmol glucose/g tissue). $n = 3–5$ mice/genotype. *B*, blood glucose levels after a 16-hour fast (mmol/liter). $n = 15–17$ mice/genotype. *C*, insulin tolerance test. $n = 8–11$ mice/genotype. *Inset*, area above the curve (*AUC*). *D*, glucose tolerance test. Glucose was injected immediately after time 0. Note the much lower blood glucose in *Epm2aip1*$^{-/-}$ mice 15 min following injection. $n = 15–17$ mice/genotype. ***, $p < 0.001$; *, $p < 0.05$. Body weights were not significantly different between genotypes. *Inset*, area under the curve (*AUC*). $p < 1 \times 10^{-4}$. *E*, endogenous (hepatic) glucose production (*EGP*) during the hyperinsulinemic-euglycemic clamp. Note lack of reduction in EGP in *Epm2aip1*$^{-/-}$ mice following insulin infusion (after time 0 min). *Left inset*, insulin values at the end of the clamp (120 min). *Right inset*, percent suppression of EGP (percentage drop in EGP during the clamp (average of the last three time points) from basal EGP levels (average of the first three time points). Lack of suppression was significant at $p < 0.007$. $n = 5–6$ mice/genotype. *F*, whole-body glucose disposal during the hyperinsulinemic-euglycemic clamp. Basal glucose disposal and disposal during insulin infusion are shown. $n = 5–6$ mice/genotype. *Avg*, average.

Base-line blood glucose, cholesterol, triglycerides, and insulin were normal in *Epm2aip1*$^{-/-}$ mice. Blood glucose following a 16-hour fast was reduced significantly (Fig. 3*B*), consistent with the low liver glycogen stores, the main stores consumed to maintain blood glucose during overnight fasts in mice (22). The insulin tolerance test (the degree of drop in blood glucose following insulin injection) was normal (Fig. 3*C*). The rate of clearance of injected glucose in the glucose tolerance test was increased (Fig. 3*D*).

*Epm2aip1*$^{-/-}$ *Mice Have Hepatic Insulin Resistance*—Reduced glycogen synthesis is a major component of insulin resistance (3–5). To determine whether *Epm2aip1*$^{-/-}$ mice are insulin-resistant, we performed a euglycemic-hyperinsulinemic clamp experiment. In this experiment, euglycemia

Downloaded from http://www.jbc.org/ by guest on January 1, 2016

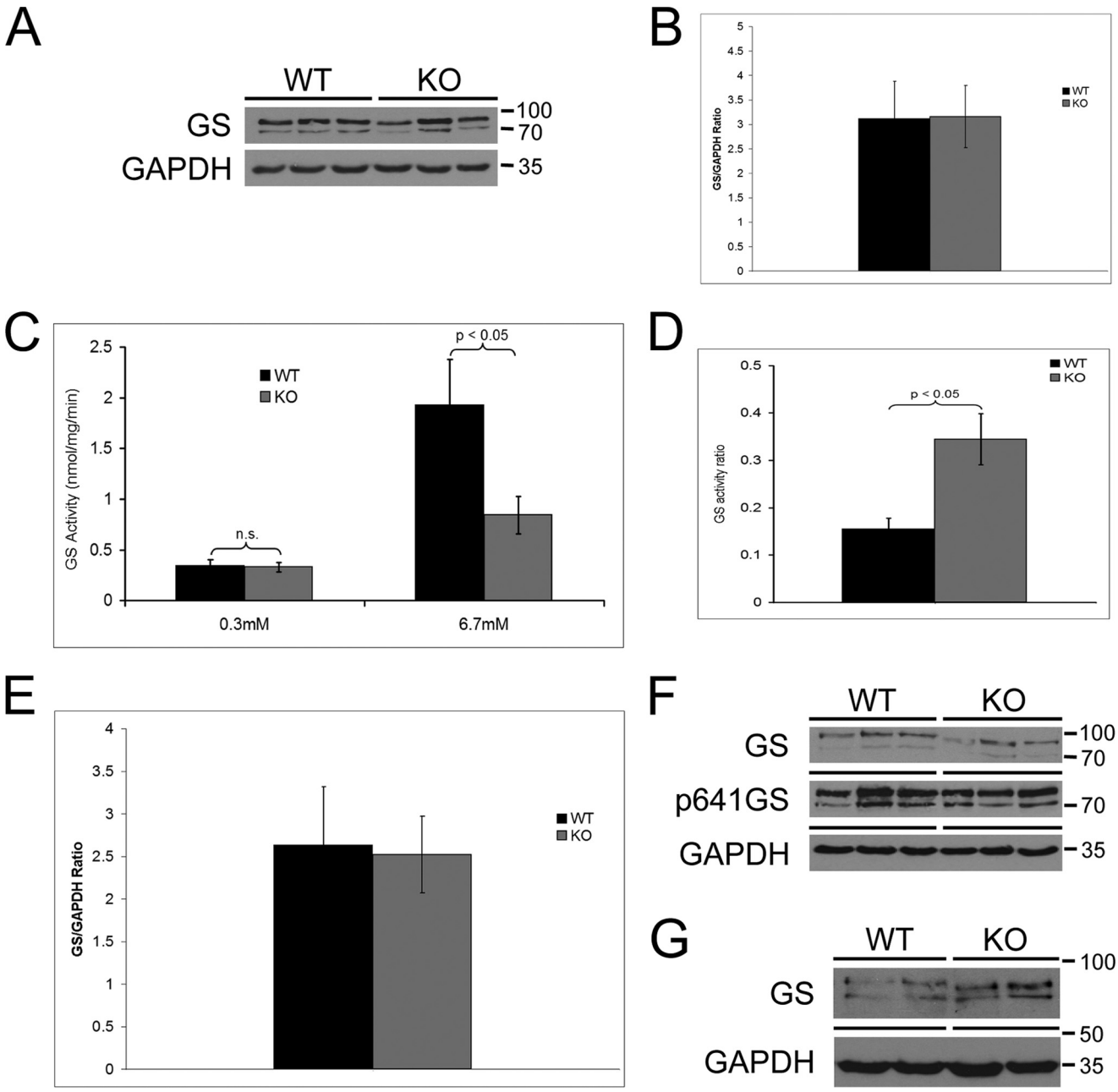


FIGURE 4. **The absence of Epm2aip1 impairs hepatic GS activation by G6P.** *A*, example Western blot analysis of hepatic GS. Note higher-phosphorylation (*top*) and lower-phosphorylation (*bottom*) bands. *B*, densitometric quantification of total hepatic GS (sums of higher-phosphorylation and lower-phosphorylation bands). Protein levels were normalized by dividing with GAPDH. $n = 5–7$ mice/genotype. *C*, hepatic GS activity at low and high G6P. $n = 8$ mice/genotype. *n.s.*, not significant. *D*, the activity ratio (GS activity at low G6P divided by GS activity at high G6P), a standard measure for reporting the active GS fraction of total possible GS activity in a sample, on the basis of the usually invariant full activation of GS by high G6P. In this situation, the latter fails, and the activity ratio is inapplicable. The ratio is high, not because GS activity at low G6P (numerator) is high but because GS activity at high G6P (denominator) is impaired. *E*, densitometric quantification of the higher-phosphorylation GS band. $n = 5–7$ mice/genotype. *F*, Western blot analysis of hepatic GS using a specific antibody against GS phosphorylated at serine 641. This antibody also is known to detect two bands, likely GS proteins with different degrees of phosphorylation outside of serine 641. Equal amounts of protein were run on two separate gels for phospho-GS (*p641GS*) and GS. *G*, Western blot analysis of hepatic GS, using the antibody against total GS, run long in a low percentage (10%) polyacrylamide gel. Note that the upper band migrates faster in *Epm2aip1*$^{-/-}$ mice.

(achieved by infusing varying amounts of glucose) and a constant amount of insulin (3 milliunits/kg/min) are maintained, and whole-body glucose utilization and endogenous glucose production are measured (28). Insulin resistance comprises impaired whole-body glucose disposal (mainly a muscle and liver function) and impaired endogenous glucose production (mainly a liver function). Of note, endogenous glucose production is highly dependent on GS activity. The liver constantly breaks down glycogen (glycogenolysis) and constructs glucose (gluconeogenesis) to supply blood glucose while, at the same time, removing excess glucose into glycogen (29, 30). The amount of glucose supplied to the blood by the liver is regulated through the rate of glycogen synthesis. How much glucose reaches the blood (endoge-

Downloaded from http://www.jbc.org/ by guest on January 1, 2016

nous glucose production) depends, in a major part, on GS activity, regulated by insulin (30).

Whole-body glucose utilization of *Epm2aip1*$^{-/-}$ mice in the clamp experiment was normal (Fig. 3*F*). Therefore, despite the rapid rate in clearing excess blood glucose in the glucose tolerance test, the overall quantity of blood glucose they are able to remove in response to insulin is unchanged.

Normally, endogenous glucose production drops precipitously during the clamp experiment (*i.e.* glucose production by the liver is suppressed) because the external glucose and insulin infusions drive hepatic GS maximally. Hepatic insulin resistance is diagnosed when this response does not occur (7, 28, 30). Our WT controls exhibited the expected normal response, whereas the *Epm2aip1*$^{-/-}$ mice had complete failure of endogenous glucose production suppression (Fig. 3*E*) and, therefore, have hepatic insulin resistance.

*Hepatic GS Activation by G6P Is Greatly Reduced in Epm2aip1*$^{-/-}$ *Mice*—Blocked hepatic glycogen synthesis at a time when it should normally be highly activated, *i.e.* during feeding after fasting or during the hyperinsulinemia of the clamp, could be explained by a deficiency in the quantity of GS or a defect in its activity or activation. GS Western blot analyses detect a double band composed of higher-phosphorylation (less active) upper and lower-phosphorylation (more active) lower bands (Fig. 4*A*) (31). We quantified total hepatic GS by quantifying the two bands together densitometrically and found no difference between *Epm2aip1*$^{-/-}$ and WT mice (Fig. 4*B*). We also quantified glycogen-bound GS following ultracentrifugation of the glycogen pellet and, again, found no differences between genotypes. GS amounts in *Epm2aip1*$^{-/-}$ livers are, therefore, not reduced.

We next examined whether there is a defect in GS activity or activation. We measured GS activity from liver extracts in the presence of low (0.3 mM) and high (6.7 mM) G6P. Activity at low G6P reflects GS activity as set by the degree of GS phosphorylation. Activity at high G6P, which overrides any inhibition through phosphorylation, indicates maximal GS activity in a particular sample (2). At low G6P, there was no difference in GS activity between *Epm2aip1*$^{-/-}$ and WT mice, but at high G6P, *Epm2aip1*$^{-/-}$ mice exhibited a major deficit in GS activity (Fig. 4, *C–D*), indicating that *Epm2aip1*$^{-/-}$ mice have a major defect in allosteric activation of GS by G6P.

We next queried whether the second arm of GS regulation, phosphorylation, is affected. The quantity of the higher-phosphorylation GS band was not increased in the *Epm2aip1*$^{-/-}$ mice (Fig. 4*E*). GS phosphorylated at serine 641, the main GSK3 phosphorylation site of GS, which reflects overall phosphorylation of the enzyme (32), was normal (Fig. 4*F*). Differences in levels of phosphorylation can be distinguished by running protein samples for longer periods of time in low-concentration gels, with more highly phosphorylated proteins migrating slower (8, 33). When we ran our Western blot analyses in this fashion we observed that the higher-phosphorylation GS band of *Epm2aip1*$^{-/-}$ mice runs faster, not slower, than its WT counterpart (Fig. 4*G*), indicating that it has reduced, not increased, phosphorylation.

The results in this section support a role for a defect in GS allosteric activation in the deficient glycogen synthesis in

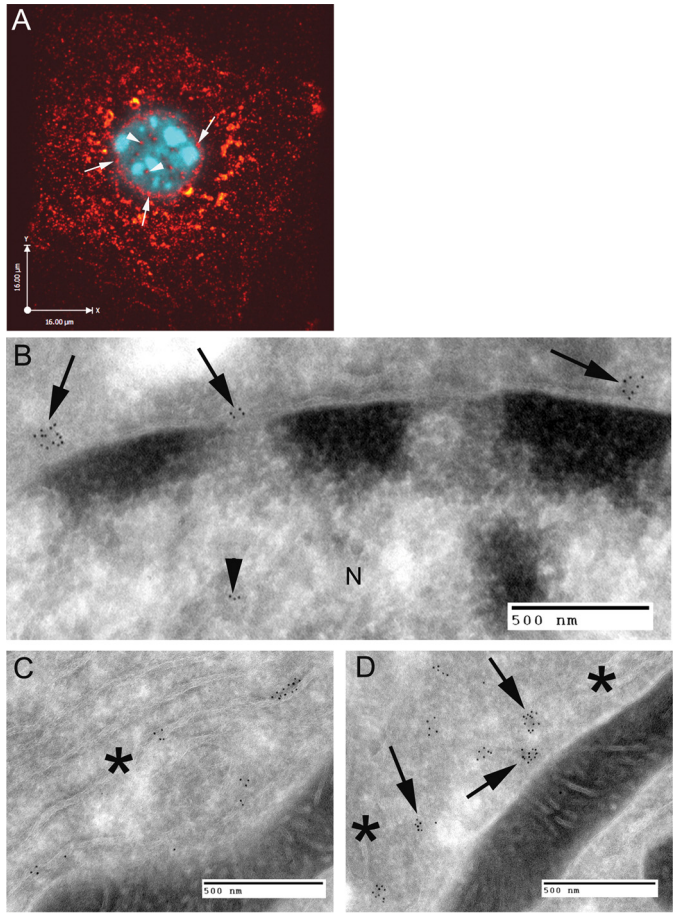


FIGURE 5. **Epm2aip1 subcellular locations.** *A*, confocal image of an immunofluorescent Epm2aip1-stained 3T3-L1 cell. Note the widespread punctate staining throughout the cytoplasm as well as in a reticular and perinuclear fashion (*arrows*). Note also the presence of the protein within the nucleus (*arrowheads*). *B*, electron micrograph of an immunogold-labeled ultrathin liver cryosection using the Epm2aip1 antibody. Note the clusters of gold particles (8 nm) in close proximity to nuclear pores (*arrows*). A cluster is also seen within the nucleus (*arrowhead*). *C*, immunogold labeling in the cytoplasm of a hepatocyte at the endoplasmic reticulum (*asterisk*). *D*, immunogold labeling in a glycogen-rich region of liver (*arrows*).

*Epm2aip1*$^{-/-}$ livers. Phosphorylation does not appear to be involved. If anything, the enzyme is hypophosphorylated, possibly a compensatory response in the face of the impaired allosterism, allowing achievement of WT GS activity levels at low G6P, but not at high G6P (Fig. 4*C*).

*Epm2aip1 Associates with GS*—Having shown that Epm2aip1 affects GS activity, we investigated whether it does so through association with the enzyme. Toward this end, we first determined the subcellular location of Epm2aip1. The protein localizes mainly in the cytoplasm (Figs. 5 and 6, *C–F*) but also in the nucleus (Fig. 5, *A* and *B*). In the cytoplasm, it is not present inside any organelle. Instead, it is distributed in glycogen-rich regions (Figs. 5*D* (from liver) and 6, *C–F* (from skeletal muscle)), and it is present at the endoplasmic reticulum (Fig. 5*C*) and at the nuclear membrane (Fig. 5, *A* and *B*), including in clusters at the nuclear membrane pores (Fig. 5*B*). Both the glycogen-rich cytoplasm and the nucleus are cell compartments in which GS is also located (2, 16).

To determine whether Epm2aip1 associates with GS, we coexpressed the two proteins in COS7 cells. Immunoprecipita-

Downloaded from http://www.jbc.org/ by guest on January 1, 2016

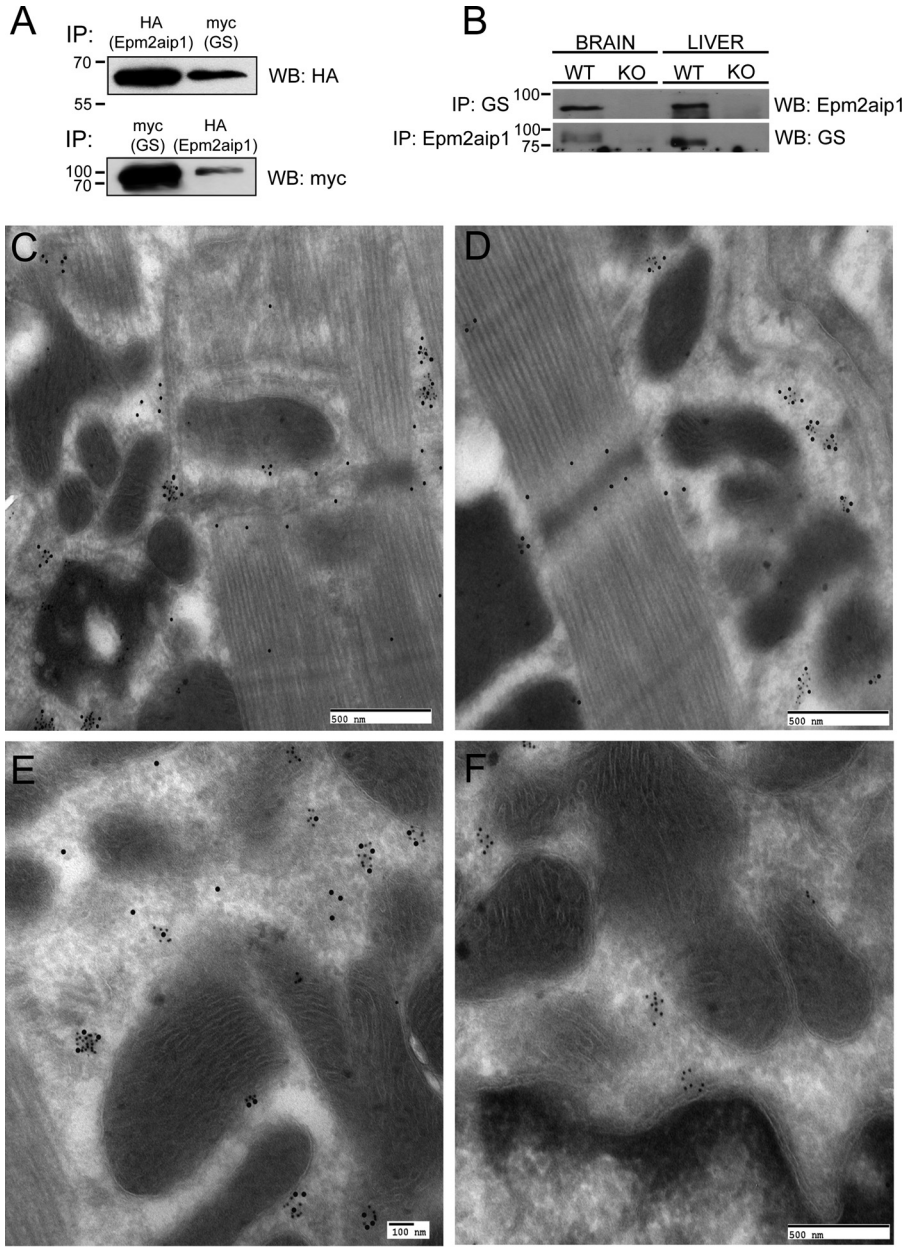


FIGURE 6. **Epm2aip1 and GS associate.** *A*, immunoprecipitation (*IP*) of Epm2aip1 by GS, and vice versa, from transfected cells. *B*, immunoprecipitation of endogenous Epm2aip1 by GS, and *vice versa*, from mouse brain and liver. *WB*, Western blot. *C*, ultrathin cryosection of skeletal muscle from WT muscle double-labeled with the Epm2aip1 (15-nm particles) and GS (8-nm particles) antibodies. Note the intense colocalization in particle clusters in the perinuclear cytoplasm and in the spaces between the sarcomeres. *D*, subsarcolemmal colocalization of Epm2aip1 and GS. *E*, colocalization of Epm2aip1 and GS in the sarcoplasm. *F*, ultrathin cryosection of skeletal muscle from an *Epm2aip1*$^{-/-}$ mouse. No Epm2aip1 signal was detected. GS was found in similar clusters to those seen in the WT mouse muscle.

tion using antibodies against one coprecipitated the other (Fig. 6*A*). Likewise, without overexpression, immunoprecipitating endogenous GS from mouse tissues coprecipitated Epm2aip1 and vice versa (Fig. 6*B*), indicating that the two proteins interact or closely associate in a complex and that, therefore, the resistance of GS to G6P activation in *Epm2aip1*$^{-/-}$ mice is likely due to loss of a direct or near-direct effect of Epm2aip1 on GS. Electron microscopy following immunogold labeling of endogenous Epm2aip1 and GS confirmed the close physical association of the two proteins (Figs. 6, *C–F*).

*Impaired Activation of GS by G6P Is Also Present in Skeletal Muscle*—Analyzing *Epm2aip1*$^{-/-}$ skeletal muscle revealed no diminution in glycogen at the base line or upon refeeding after fasting, the latter not unexpected because fasting alone does not significantly reduce muscle glycogen (34) and did not do so in these animals. The total quantity of GS and the fraction of GS associated with glycogen were also normal.

GS activation by G6P was not impaired, although there appeared to be a possible trend (Figs. 7, *A* and *B*). Noting the latter, we took an additional step and asked whether G6P activation of GS might be significantly abnormal under conditions where GS is maximally active. We fasted the mice for 16 h, ran them on a treadmill until exhaustion, which greatly reduces muscle glycogen (34), and then refed them for 1 h before sacrifice, *i.e.* the mice were sacrificed in the midst of maximal glycogen resynthesis. Under these conditions, we observed a robustly significant

Downloaded from http://www.jbc.org/ by guest on January 1, 2016

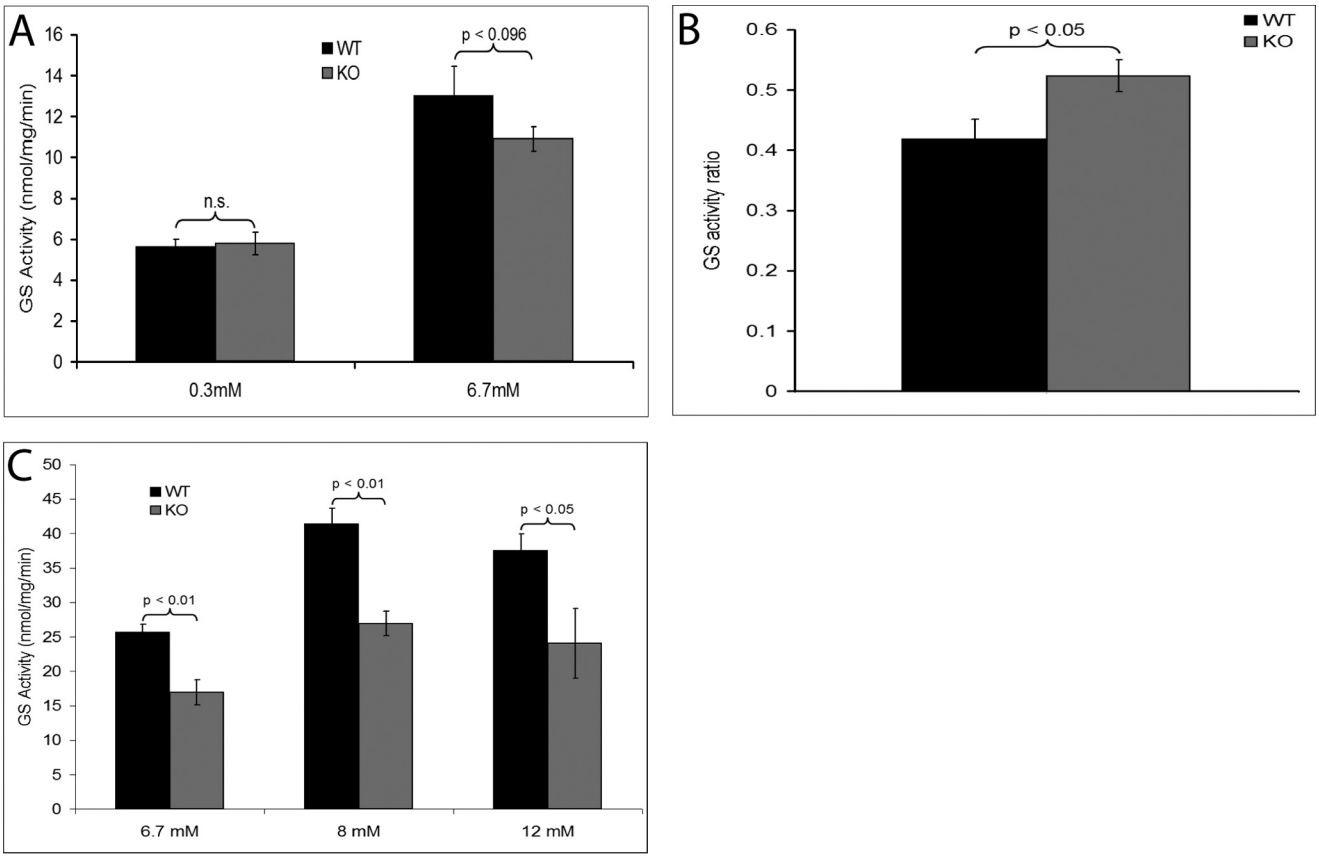


FIGURE 7. **GS activation by G6P is also impaired in skeletal muscle.** *A*, skeletal muscle GS activity with low and high G6P. $n = 6$ mice/genotype. *n.s.*, not significant. *B*, GS activity ratio of the results in *A*: GS activity at low G6P divided by that at high G6P. Note that the activity ratio is high, not because the activity at low G6P is high but because the activity at high G6P, *i.e.* the ability of G6P to activate GS, is low. $n = 6$ mice/genotype. *C*, skeletal muscle GS activity at 1-h refeeding following glycogen depletion by fasting and exhaustive exercise. $n = 6$ mice/genotype.

reduction in the ability of G6P to activate GS in *Epm2aip1*$^{-/-}$ mice (Fig. 7*C*), confirming that the effect of Epm2aip1 absence on GS activation in liver is also present in skeletal muscle.

*Epm2aip1*$^{-/-}$ *Mice Are Resistant to Age-dependent Obesity*—As mentioned, GS has two isoforms, one specific to liver (GYS2), the other to skeletal muscle and other tissues (GYS1) (2). As discussed below, many features of the *Epm2aip1*$^{-/-}$ mice are shared between mice lacking Gys2 (LGSKO) (22) and mice lacking Gys1 (MGSKO) (35). Normally, adult laboratory mice fed standard chow gain weight and become obese with age, which is true of LGSKO mice (22) but not of MGSKO mice. The latter did not gain weight in adult life, despite consuming normal amounts of food (35). To determine whether adult *Epm2aip1*$^{-/-}$ mice gain weight with age in adulthood, we weighed a group of mice every 2 months over 1 year. Between 2 and 12 months, WT animals gained an average of 22.44 ± 3.60 g, whereas *Epm2aip1*$^{-/-}$ mice gained only 9.85 ± 1.24 g (Fig. 8). The amount of food consumed by the two genotypes was the same (*Epm2aip1*$^{-/-}$, 0.21 ± 0.03; WT, 0.23 ± 0.07 g/day/g body weight). *Epm2aip1*$^{-/-}$ mice are therefore, like MGSKO mice, resistant to age-related weight gain in adulthood.

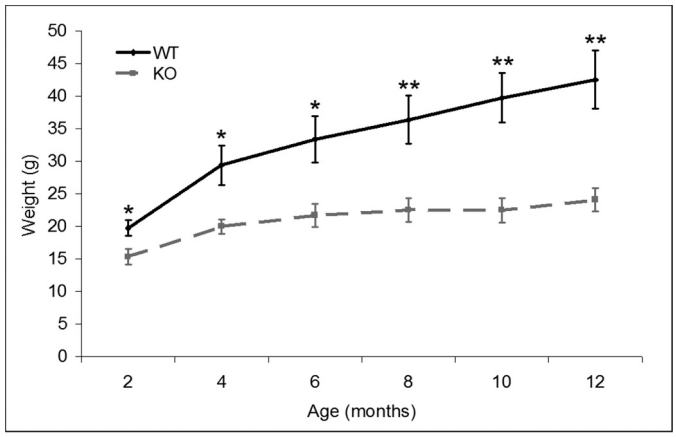


FIGURE 8. **Epm2aip1**$^{-/-}$ **mice exhibit an absence of weight gain with age in adulthood.** $n = 5–6$ mice/genotype. *, $p < 0.05$; **, $p < 0.01$.

## DISCUSSION

Insulin moves glucose entering the circulation into appropriate storage and processing. At the same time, and equally importantly, it suppresses endogenous glucose production and secretion into the bloodstream, primarily by increasing hepatic glycogen synthesis. Insulin resistance comprises impaired glucose disposal and impaired suppression of glucose secretion. Identifying the proteins involved in these processes is, therefore, critical to understanding insulin resistance. The two principal glucose disposal tissues are skeletal muscle and liver. Knockout of the insulin receptor, or of GS, from mouse skeletal muscle alone has little or no impact on whole-body glucose disposal even while affecting muscle glucose disposal (35–38).

Downloaded from http://www.jbc.org/ by guest on January 1, 2016

Removal of the insulin receptor, or GS, from the liver alone impairs the suppression of endogenous glucose provision to the blood and causes hepatic insulin resistance (22, 39). We identified a ubiquitously expressed protein, Epm2aip1, that associates with GS and whose absence impairs GS activation and causes hepatic insulin resistance.

*Epm2aip1*$^{-/-}$ mice share features of LGSKO mice (22), including reduced hepatic glycogen synthesis, hepatic insulin resistance, fasting hypoglycemia, and hepatic fat accumulation, the latter occurring earlier in *Epm2aip1*$^{-/-}$ (at 2 months) than in LGSKO (at 7 months). Reduced hepatic glycogen synthesis, hepatic insulin resistance, and hepatic fat accumulation also occur with disturbances of hepatic insulin signaling. When the insulin receptor, or its downstream signaling substrates Irs1 and Irs2, were completely removed from mouse liver, glycogen synthesis was greatly reduced, with no associated lipid accumulation (39, 40), but when Irs1 and Irs2 were down-regulated but not eliminated, glycogen synthesis was partially reduced, and hepatic lipid accumulation occurred at 2 months of age (41). Thus, the effect of absent Epm2aip1 on hepatic glycogenesis and lipogenesis is most similar to that of partial impairment of hepatic insulin signaling.

*Epm2aip1*$^{-/-}$ mice also share features of MGSKO mice (35), namely resistance against age-dependent obesity and a rapid rate of clearance of exogenous glucose. The mechanisms underlying the former remain unknown. Results in MGSKO mice preliminarily suggest heightened oxidative capacity (35). Uncovering these mechanisms in MGSKO and *Epm2aip1*$^{-/-}$ mice is of obvious importance. The rapid rate of glucose clearance in response to a rise in glucose is also unexplained but may reflect an increased ability to dispose of glucose via insulin-independent mechanisms, *i.e.* increased glucose effectiveness (42). Neither MGSKO (35) nor *Epm2aip1*$^{-/-}$ or LGSKO mice (22) have reduced whole-body glucose utilization in response to insulin, indicating that partial loss of glycogen synthesis through complete loss in only muscle (MGSKO) or in only liver (LGSKO) or through partial loss across both organs (*Epm2aip1*$^{-/-}$) does not, alone, suffice to affect the overall ability of insulin to clear glucose from the blood.

Although it has long been known that allosteric activation of GS is far more potent than dephosphorylation *in vitro*, it was not confirmed *in vivo* until recently. Mutating a key amino acid in the GS allosteric site led to 80% loss of insulin-mediated glycogen synthesis without alteration of the phosphorylation of the enzyme (36). In this work, we identify a protein, Epm2aip1, that modulates the allosteric response of GS to G6P, possibly through direct action given its association with GS. Its action appears to not involve phosphoregulation because the inhibited enzyme in its absence is hypophosphorylated. Finally, in the absence of Epm2aip1, the sensitivity of the liver to insulin, in which GS is a principal actor, is impaired. Until now, the only known way by which insulin regulates the allosteric action of GS by G6P is through increasing the amount of G6P. In liver, although glucokinase and glucose 6-phosphatase are subject to non-transcriptional regulation during refeeding (43–45), the only known mechanism whereby insulin itself affects these enzymes and increases G6P are transcriptional, *e.g.* increasing glucokinase expression (6, 46). The immediacy of insulin action on glycogen synthesis likely requires non-transcriptional mechanisms. GS in tissues of patients with type 2 diabetes has reduced activity and is hyperphosphorylated (2, 8–10, 47). The latter observation focused searches for pathomechanisms of type 2 diabetes on disturbances affecting the phosphorylation of the enzyme. Although part of the answer to insulin resistance must involve GS phosphorylation, the literature is equally replete with evidence that, in type 2 diabetics, allosteric activation of GS by G6P is also impaired to a major degree (48–52). Uncovering the molecular components underlying this failure is important in understanding insulin resistance. The mice studied here, lacking the Epm2aip1 protein, have failed GS allosteric activation and hepatic insulin resistance. Epm2aip1, which associates with GS, may, therefore, be a modulator of GS allosterism under insulin control. Its precise mode of action and regulation awaits further study.

*Acknowledgments—We thank Drs. J. Rommens and S. Meyn for review of our manuscript.*

## REFERENCES


1. Acheson, K. J., Schutz, Y., Bessard, T., Anantharaman, K., Flatt, J. P., and Jéquier, E. (1988) Glycogen storage capacity and *de novo* lipogenesis during massive carbohydrate overfeeding in man. *Am. J. Clin. Nutr.* **48,** 240–247
2. Roach, P. J. (2002) Glycogen and its metabolism. *Curr. Mol. Med.* **2,** 101–120
3. Damsbo, P., Vaag, A., Hother-Nielsen, O., and Beck-Nielsen, H. (1991) Reduced glycogen synthase activity in skeletal muscle from obese patients with and without type 2 (non-insulin-dependent) diabetes mellitus. *Diabetologia* **34,** 239–245
4. Shulman, G. I., Rothman, D. L., Jue, T., Stein, P., DeFronzo, R. A., and Shulman, R. G. (1990) Quantitation of muscle glycogen synthesis in normal subjects and subjects with non-insulin-dependent diabetes by 13C nuclear magnetic resonance spectroscopy. *N. Engl. J. Med.* **322,** 223–228
5. Thorburn, A. W., Gumbiner, B., Bulacan, F., Wallace, P., and Henry, R. R. (1990) Intracellular glucose oxidation and glycogen synthase activity are reduced in non-insulin-dependent (type II) diabetes independent of impaired glucose uptake. *J. Clin. Invest.* **85,** 522–529
6. Iynedjian, P. B. (2009) Molecular physiology of mammalian glucokinase. *Cell. Mol. Life Sci.* **66,** 27–42
7. Taylor, R., and Shulman, G. I. (2011) *Handbook of Physiology, the Endocrine System, the Endocrine Pancreas and Regulation of Metabolism*, pp. 787–802, Wiley, New York
8. Højlund, K., Birk, J. B., Klein, D. K., Levin, K., Rose, A. J., Hansen, B. F., Nielsen, J. N., Beck-Nielsen, H., and Wojtaszewski, J. F. (2009) Dysregulation of glycogen synthase COOH- and NH2-terminal phosphorylation by insulin in obesity and type 2 diabetes mellitus. *J. Clin. Endocrinol. Metab.* **94,** 4547–4556
9. Cohen, P. (1999) The Croonian Lecture 1998. Identification of a protein kinase cascade of major importance in insulin signal transduction. *Philos. Trans. R Soc. Lond. B Biol. Sci.* **354,** 485–495
10. Jensen, J., and Lai, Y. C. (2009) Regulation of muscle glycogen synthase phosphorylation and kinetic properties by insulin, exercise, adrenaline and role in insulin resistance. *Arch. Physiol. Biochem.* **115,** 13–21
11. Fong, N. M., Jensen, T. C., Shah, A. S., Parekh, N. N., Saltiel, A. R., and Brady, M. J. (2000) Identification of binding sites on protein targeting to glycogen for enzymes of glycogen metabolism. *J. Biol. Chem.* **275,** 35034–35039
12. Bruno, C., van Diggelen, O. P., Cassandrini, D., Gimpelev, M., Giuffrè, B., Donati, M. A., Introvini, P., Alegria, A., Assereto, S., Morandi, L., Mora, M., Tonoli, E., Mascelli, S., Traverso, M., Pasquini, E., Bado, M., Vilarinho, L., van Noort, G., Mosca, F., DiMauro, S., Zara, F., and Minetti, C. (2004)


Downloaded from http://www.jbc.org/ by guest on January 1, 2016

Clinical and genetic heterogeneity of branching enzyme deficiency (glycogenosis type IV). *Neurology* **63,** 1053–1058
13. Minassian, B. A., Lee, J. R., Herbrick, J. A., Huizenga, J., Soder, S., Mungall, A. J., Dunham, I., Gardner, R., Fong, C. Y., Carpenter, S., Jardim, L., Satishchandra, P., Andermann, E., Snead, O. C., 3rd, Lopes-Cendes, I., Tsui, L. C., Delgado-Escueta, A. V., Rouleau, G. A., and Scherer, S. W. (1998) Mutations in a gene encoding a novel protein tyrosine phosphatase cause progressive myoclonus epilepsy. *Nat. Genet.* **20,** 171–174
14. Tagliabracci, V. S., Girard, J. M., Segvich, D., Meyer, C., Turnbull, J., Zhao, X., Minassian, B. A., Depaoli-Roach, A. A., and Roach, P. J. (2008) Abnormal metabolism of glycogen phosphate as a cause for Lafora disease. *J. Biol. Chem.* **283,** 33816–33825
15. Chan, E. M., Young, E. J., Ianzano, L., Munteanu, I., Zhao, X., Christopoulos, C. C., Avanzini, G., Elia, M., Ackerley, C. A., Jovic, N. J., Bohlega, S., Andermann, E., Rouleau, G. A., Delgado-Escueta, A. V., Minassian, B. A., and Scherer, S. W. (2003) Mutations in NHLRC1 cause progressive myoclonus epilepsy. *Nat. Genet.* **35,** 125–127
16. Vilchez, D., Ros, S., Cifuentes, D., Pujadas, L., Vallès, J., García-Fojeda, B., Criado-García, O., Fernández-Sánchez, E., Medraño-Fernández, I., Domínguez, J., García-Rocha, M., Soriano, E., Rodríguez de Córdoba, S., and Guinovart, J. J. (2007) Mechanism suppressing glycogen synthesis in neurons and its demise in progressive myoclonus epilepsy. *Nat. Neurosci.* **10,** 1407–1413
17. Valles-Ortega, J., Duran, J., Garcia-Rocha, M., Bosch, C., Saez, I., Pujadas, L., Serafin, A., Cañas, X., Soriano, E., Delgado-García, J. M., Gruart, A., and Guinovart, J. J. (2011) Neurodegeneration and functional impairments associated with glycogen synthase accumulation in a mouse model of Lafora disease. *EMBO Mol. Med.* **3,** 667–681
18. Turnbull, J., Wang, P., Girard, J. M., Ruggieri, A., Wang, T. J., Draginov, A. G., Kameka, A. P., Pencea, N., Zhao, X., Ackerley, C. A., and Minassian, B. A. (2010) Glycogen hyperphosphorylation underlies Lafora body formation. *Ann. Neurol.* **68,** 925–933
19. Ianzano, L., Zhao, X. C., Minassian, B. A., and Scherer, S. W. (2003) Identification of a novel protein interacting with laforin, the EPM2a progressive myoclonus epilepsy gene product. *Genomics* **81,** 579–587
20. Turnbull, J., Girard, J. M., Lohi, H., Chan, E. M., Wang, P., Tiberia, E., Omer, S., Ahmed, M., Bennett, C., Chakrabarty, A., Tyagi, A., Liu, Y., Pencea, N., Zhao, X., Scherer, S. W., Ackerley, C. A., and Minassian, B. A. (2012) Early-onset Lafora body disease. *Brain* **135,** 2684–2698
21. Niederwanger, A., Kranebitter, M., Ritsch, A., Patsch, J. R., and Pedrini, M. T. (2005) A gel filtration assay to determine glycogen synthase activity. *J. Chromatogr. B Analyt. Technol. Biomed. Life Sci.* **820,** 143–145
22. Irimia, J. M., Meyer, C. M., Peper, C. L., Zhai, L., Bock, C. B., Previs, S. F., McGuinness, O. P., DePaoli-Roach, A., and Roach, P. J. (2010) Impaired glucose tolerance and predisposition to the fasted state in liver glycogen synthase knock-out mice. *J. Biol. Chem.* **285,** 12851–12861
23. Tourlakis, M. E., Zhong, J., Gandhi, R., Zhang, S., Chen, L., Durie, P. R., and Rommens, J. M. (2012) Deficiency of Sbds in the mouse pancreas leads to features of Shwachman-Diamond syndrome, with loss of zymogen granules. *Gastroenterology* **143,** 481–492
24. Duez, H., Smith, A. C., Xiao, C., Giacca, A., Szeto, L., Drucker, D. J., and Lewis, G. F. (2009) Acute dipeptidyl peptidase-4 inhibition rapidly enhances insulin-mediated suppression of endogenous glucose production in mice. *Endocrinology* **150,** 56–62
25. DePaoli-Roach, A. A., Tagliabracci, V. S., Segvich, D. M., Meyer, C. M., Irimia, J. M., and Roach, P. J. (2010) Genetic depletion of the malin E3 ubiquitin ligase in mice leads to Lafora bodies and the accumulation of insoluble laforin. *J. Biol. Chem.* **285,** 25372–25381
26. Ganesh, S., Delgado-Escueta, A. V., Sakamoto, T., Avila, M. R., Machado-Salas, J., Hoshii, Y., Akagi, T., Gomi, H., Suzuki, T., Amano, K., Agarwala, K. L., Hasegawa, Y., Bai, D. S., Ishihara, T., Hashikawa, T., Itohara, S., Cornford, E. M., Niki, H., and Yamakawa, K. (2002) Targeted disruption of the Epm2a gene causes formation of Lafora inclusion bodies, neurodegeneration, ataxia, myoclonus epilepsy and impaired behavioral response in mice. *Hum. Mol. Genet.* **11,** 1251–1262
27. Chen, C., Williams, P. F., and Caterson, I. D. (1993) Liver and peripheral tissue glycogen metabolism in obese mice. Effect of a mixed meal. *Am. J. Physiol.* **265,** E743–E751
28. Kim, J. K. (2009) Hyperinsulinemic-euglycemic clamp to assess insulin sensitivity *in vivo*. *Methods Mol. Biol.* **560,** 221–238
29. Jungermann, K., and Kietzmann, T. (1996) Zonation of parenchymal and nonparenchymal metabolism in liver. *Annu. Rev. Nutr.* **16,** 179–203
30. Petersen, K. F., Laurent, D., Rothman, D. L., Cline, G. W., and Shulman, G. I. (1998) Mechanism by which glucose and insulin inhibit net hepatic glycogenolysis in humans. *J. Clin. Invest.* **101,** 1203–1209
31. Kadotani, A., Fujimura, M., Nakamura, T., Ohyama, S., Harada, N., Maruki, H., Tamai, Y., Kanatani, A., Eiki, J., and Nagata, Y. (2007) Metabolic impact of overexpression of liver glycogen synthase with serine-to-alanine substitutions in rat primary hepatocytes. *Arch. Biochem. Biophys.* **466,** 283–289
32. Skurat, A. V., and Roach, P. J. (2004) *Diabetes Mellitus. A Fundamental and Clinical Text* (Leroith, D., and Taylor, S. I., eds), Lippincott Williams & Wilkins, Philadelphia
33. Printen, J. A., Brady, M. J., and Saltiel, A. R. (1997) PTG, a protein phosphatase 1-binding protein with a role in glycogen metabolism. *Science* **275,** 1475–1478
34. Pederson, B. A., Cope, C. R., Schroeder, J. M., Smith, M. W., Irimia, J. M., Thurberg, B. L., DePaoli-Roach, A. A., and Roach, P. J. (2005) Exercise capacity of mice genetically lacking muscle glycogen synthase. In mice, muscle glycogen is not essential for exercise. *J. Biol. Chem.* **280,** 17260–17265
35. Pederson, B. A., Schroeder, J. M., Parker, G. E., Smith, M. W., DePaoli-Roach, A. A., and Roach, P. J. (2005) Glucose metabolism in mice lacking muscle glycogen synthase. *Diabetes* **54,** 3466–3473
36. Bouskila, M., Hunter, R. W., Ibrahim, A. F., Delattre, L., Peggie, M., van Diepen, J. A., Voshol, P. J., Jensen, J., and Sakamoto, K. (2010) Allosteric regulation of glycogen synthase controls glycogen synthesis in muscle. *Cell Metab.* **12,** 456–466
37. Brüning, J. C., Michael, M. D., Winnay, J. N., Hayashi, T., Hörsch, D., Accili, D., Goodyear, L. J., and Kahn, C. R. (1998) A muscle-specific insulin receptor knockout exhibits features of the metabolic syndrome of NIDDM without altering glucose tolerance. *Mol. Cell* **2,** 559–569
38. Kim, J. K., Michael, M. D., Previs, S. F., Peroni, O. D., Mauvais-Jarvis, F., Neschen, S., Kahn, B. B., Kahn, C. R., and Shulman, G. I. (2000) Redistribution of substrates to adipose tissue promotes obesity in mice with selective insulin resistance in muscle. *J. Clin. Invest.* **105,** 1791–1797
39. Michael, M. D., Kulkarni, R. N., Postic, C., Previs, S. F., Shulman, G. I., Magnuson, M. A., and Kahn, C. R. (2000) Loss of insulin signaling in hepatocytes leads to severe insulin resistance and progressive hepatic dysfunction. *Mol. Cell* **6,** 87–97
40. Kubota, N., Kubota, T., Itoh, S., Kumagai, H., Kozono, H., Takamoto, I., Mineyama, T., Ogata, H., Tokuyama, K., Ohsugi, M., Sasako, T., Moroi, M., Sugi, K., Kakuta, S., Iwakura, Y., Noda, T., Ohnishi, S., Nagai, R., Tobe, K., Terauchi, Y., Ueki, K., and Kadowaki, T. (2008) Dynamic functional relay between insulin receptor substrate 1 and 2 in hepatic insulin signaling during fasting and feeding. *Cell Metab.* **8,** 49–64
41. Taniguchi, C. M., Ueki, K., and Kahn, R. (2005) Complementary roles of IRS-1 and IRS-2 in the hepatic regulation of metabolism. *J. Clin. Invest.* **115,** 718–727
42. Best, J. D., Kahn, S. E., Ader, M., Watanabe, R. M., Ni, T. C., and Bergman, R. N. (1996) Role of glucose effectiveness in the determination of glucose tolerance. *Diabetes Care* **19,** 1018–1030
43. Agius, L., Peak, M., Newgard, C. B., Gomez-Foix, A. M., and Guinovart, J. J. (1996) Evidence for a role of glucose-induced translocation of glucokinase in the control of hepatic glycogen synthesis. *J. Biol. Chem.* **271,** 30479–30486
44. Daniele, N., Rajas, F., Payrastre, B., Mauco, G., Zitoun, C., and Mithieux, G. (1999) Phosphatidylinositol 3-kinase translocates onto liver endoplasmic reticulum and may account for the inhibition of glucose-6-phosphatase during refeeding. *J. Biol. Chem.* **274,** 3597–3601
45. Newgard, C. B., Foster, D. W., and McGarry, J. D. (1984) Evidence for suppression of hepatic glucose-6-phosphatase with carbohydrate feeding. *Diabetes* **33,** 192–195
46. Dong, X. C., Copps, K. D., Guo, S., Li, Y., Kollipara, R., DePinho, R. A., and White, M. F. (2008) Inactivation of hepatic Foxo1 by insulin signaling is required for adaptive nutrient homeostasis and endocrine growth regulation. *Cell Metab.* **8,** 65–76

Downloaded from http://www.jbc.org/ by guest on January 1, 2016

47. Nikoulina, S. E., Ciaraldi, T. P., Mudaliar, S., Mohideen, P., Carter, L., and Henry, R. R. (2000) Potential role of glycogen synthase kinase-3 in skeletal muscle insulin resistance of type 2 diabetes. *Diabetes* **49,** 263–271
48. Golay, A., Munger, R., Assimacopoulos-Jeannet, F., Bobbioni-Harsch, E., Habicht, F., and Felber, J. P. (2002) Progressive defect of insulin action on glycogen synthase in obesity and diabetes. *Metabolism* **51,** 549–553
49. Golay, A., and Ybarra, J. (2005) Link between obesity and type 2 diabetes. *Best Pract. Res. Clin. Endocrinol. Metab.* **19,** 649–663
50. Henry, R. R., Ciaraldi, T. P., Abrams-Carter, L., Mudaliar, S., Park, K. S., and Nikoulina, S. E. (1996) Glycogen synthase activity is reduced in cultured skeletal muscle cells of non-insulin-dependent diabetes mellitus subjects. Biochemical and molecular mechanisms. *J. Clin. Invest.* **98,** 1231–1236
51. Meyer, M. M., Levin, K., Grimmsmann, T., Beck-Nielsen, H., and Klein, H. H. (2002) Insulin signalling in skeletal muscle of subjects with or without type II-diabetes and first degree relatives of patients with the disease. *Diabetologia* **45,** 813–822
52. Thorburn, A. W., Gumbiner, B., Bulacan, F., Brechtel, G., and Henry, R. R. (1991) Multiple defects in muscle glycogen synthase activity contribute to reduced glycogen synthesis in non-insulin dependent diabetes mellitus. *J. Clin. Invest.* **87,** 489–495

Downloaded from http://www.jbc.org/ by guest on January 1, 2016

**Supplementary methods and data**

**Supplementary methods – Behavioural tests**

For open field test, mice were placed in the center for 20 min, tracked by camera linked to a computer system using LimeLight software (Coulbourn Instruments, Allentown, PA), and the time in each zone (s): 1- outside, 2-middle, 3-center & total distance travelled (cm) measured.

To measure startle response, an acoustic startle reflex system (Med Associates Inc. St. Albans, VT) was used. Four standard cages were placed in sound-attenuated chambers with each cage being a Plexiglas cylinder 3cm in diameter, mounted on a platform connected to an analogue-digital converter. Background noise and acoustic bursts were conveyed through two speakers placed in proximity to the startle. Both speakers and startle cages were connected to a main PC, which detected and analyzed all chamber variables with custom software. Mice were acclimatized to apparatus for 5 minutes then presented with 80 startle stimuli (120 dB noise bursts) with an inter-stimulus interval of 15 s (background noise was 68 dB throughout session) and startle amplitude (V) measured.

Pre pulse inhibition apparatus was same as used in startle response tests. A 5-minute acclimation period, during which only the 68 dB background noise was presented, then a set of 20 startle stimuli (120 dB, 40 ms long, 15 s interval) followed by the prepulse session consisting of 90 trials each having a 20 ms pre-pulse tone, a 40 ms startle tone of 120 dB and a 100 ms inter-tone interval (onset to onset). There were 3 different pre-pulse tone amplitudes: 70, 75, 80 dB as well as no stimulus (0 dB) trials and startle alone (120 dB) trials, each presented 10 times. Inter-trial interval was 15 sec. The maximum startle response (Vmax) was measured during a 40-ms sampling window after presentation of the 120 dB startle tone. The percent of prepulse inhibition was calculated as 100 – [(average Vmax of prepulse trials/ average Vmax of startle alone trials) x 100] for each prepulse level.

For rotarod tests, mice were habituated to the procedure on day 0, each trained until all met the criteria of 1 min at a constant speed of 4rpm (if not reached, mice were removed from the study). 3 days of testing followed with 3 trials per day using an accelerated rotarod protocol (4 to 40 rpm over 10 min). Mean time to fall (s) on each test day was measured.

To measure foot splay, mouse feet were dipped in ink and the mouse was dropped from 30 cm onto a blank paper (1). The distance between feet (cm) was measured from 2 trials averaged.

To test gait, mice trained to run through a passage to a goal box for 2 days. The next day, they were tested by dipping feet in ink (forepaws and hindpaws tested separately) and the base width and stride length measured (4 largest measurements for each averaged) (2).

The grid test was performed by placing mice on a 40cmx40cm grid with 15x15mm squares, and videotaping while walking on grid for 3 minutes. The number of hind paw slips were counted for each mouse (3).

For hanging grip, mice were held at the base of the tail and allowed to grasp the rod with their front paws. They were suspended 30 cm, and 3 trials were performed on 1 day (max time per trial 60 sec). The time to drop (s) was measured for each mouse (4).

For negative geotaxis, mice were placed on a platform at a 45 degree incline. The mean time to turn around 180 degrees was measured (4).

Fear conditioning experiments were conducted in a windowless room containing 4 stainless steel conditioning chambers (31 cm × 24 cm × 21 cm; Med Associates, St. Albans, VT), containing a stainless

steel shock-grid floor. Shock grid bars (diameter 3.2 mm) were spaced 7.9 mm apart. The grid floor was positioned over a stainless-steel drop-pan, which was lightly cleaned with 70% ethyl alcohol to provide a background odour. The front, top, and back of the chamber were made of clear acrylic and the two sides made of modular aluminum. Day 1- training consisted of placing mice in a conditioning chamber and, two min later, presenting a tone (2800 Hz, 30 s, 85 dB) that co-terminated with a shock (2 s, 0.6 mA). Mice remained in the chamber for 30 s after shock delivery. Day 2- context test: returned to context for 5 minutes. Day 3- cue (tone) test: Mice were placed in a novel chamber and two min later, the tone was presented for 3 min. The index of memory (freezing behaviour) was monitored via four overhead cameras. Freezing was assessed using an automated scoring system (Actimetrics, Wilmette, IL), which digitized the video signal at 4 Hz and compared movement frame by frame to determine the amount of freezing.

For the Morris water maze test, a circular water maze tank (120 cm in diameter, 50 cm deep), located in a dimly-lit room was used. The pool was filled to a depth of 40 cm with water made opaque by adding white, nontoxic paint. Water temperature was maintained at 28 ± 1°C by a heating pad beneath the pool. A circular escape platform (10 cm diameter) was submerged 0.5 cm below the water surface, in a fixed position in one quadrant. The pool was surrounded by curtains, at least 1 m from the perimeter of the pool. The curtains were white with distinct cues painted on them. Prior to commencing training, mice were individually handled for 2 min each day over seven consecutive days. Mice were trained over five days. On each training day, mice received six training trials (presented in two blocks of three trials; interblock interval was 1 h, intertrial interval was 15 s). On each trial they were placed into the pool, facing the wall, in one of four start locations. The order of these start locations was pseudorandomly varied throughout training. The trial was complete once the mouse found the platform or 60 s had elapsed. If the mouse failed to find the platform on a given trial, the experimenter guided the mouse onto the platform. Following the completion of training, spatial memory was assessed in a probe test the next day. In this test the platform was removed from the pool, and the mouse was allowed 60 s to search for it. Behavioral data from training and the probe tests were acquired and analyzed using an automated tracking system (Actimetrics, Wilmette, IL). Measurements were made of time to reach platform (a measure of learning across days) during training. During in probe testing, performance was quantified by the amount of time mice searched the target zone (20 cm radius, centered on the location of the platform during training) vs. the average of three other equivalent zones in other areas of the pool. These zones each represent approximately 11% of the total pool surface (a measure of memory for platform location) (5).

**Supplementary References**


1. Mohammad, F. K., Faris, G. A., Rhayma, M. S., and Ahmed, K. (2006) *Neurotoxicology* **27**, 153-157
2. Iancu, R., Mohapel, P., Brundin, P., and Paul, G. (2005) *Behav Brain Res* **162**, 1-10
3. Starkey, M. L., Barritt, A. W., Yip, P. K., Davies, M., Hamers, F. P., McMahon, S. B., and Bradbury, E. J. (2005) *Exp Neurol* **195**, 524-539
4. Rogers, E. H., Hunter, E. S., 3rd, Moser, V. C., Phillips, P. M., Herkovits, J., Munoz, L., Hall, L. L., and Chernoff, N. (2005) *J Appl Toxicol* **25**, 527-534
5. Stone, S. S., Teixeira, C. M., Zaslavsky, K., Wheeler, A. L., Martinez-Canabal, A., Wang, A. H., Sakaguchi, M., Lozano, A. M., and Frankland, P. W. (2010) *Hippocampus* **Epub: 2010/09/09**


**Supplementary figure 1. Neurobehavioral testing of *Epm2aip1*$^{-/-}$ mice.**

(A–B) Open field test. Measure of anxiety by measuring time spent in each zone (seconds) and total distance traveled in cm; n = 10 per genotype.

(C) Acoustic startle response. Reflex to protective startle in response to a sudden acoustic stimulus, displayed as mean startle amplitude (V). n = 10 per genotype.

(D) Prepulse inhibition. Sensorimotor gating measurement using % of prepulse inhibition; n = 10 per genotype.

(E–F) Fear conditioning. Context and cue (tone) fear memory to determine amount of freezing (% time spent freezing); n = 10 per genotype.

(G–H) Morris water maze. Spatial memory test showing time to reach platform (training) and amount of time spent searching for target zone (probe); n = 10 per genotype.

**Supplementary figure 2. Neuromotor testing in *Epm2aip1*$^{-/-}$ mice.**

(A) Rotarod. Motor coordination and/or fatigue shown by mean time to fall on each test day (seconds). Parametric ANOVA statistical analyses also showed significant differences among genotypes; $p < 0.05$; n = 10 per genotype.
(B) Grid test. Deficits in voluntary motor control shown by number of hind paw slips per mouse; n = 10 per genotype.
(C) Hanging grip test. Muscle strength measured by time to drop (seconds); n = 10 per genotype.
(D) Negative geotaxis. Neuromotor coordination tested by calculating time for each mouse to turn around 180 degrees after being placed facing downwards; n = 10 per genotype.
(E) Foot splay analysis. Evaluation of peripheral neuropathy and/or central nervous system depression by measuring distance between splayed feet after dropping from a height of 30 cm; n = 10 per genotype.

**Supplementary figure 3. Gait testing in *Epm2aip1*$^{-/-}$ mice.**

(A–B) Forelimb gait analysis. Motor impairment tested by measuring stride length and base width (distance between foot prints in cm); n = 10 per genotype.

(C–D) Hindlimb gait analysis. Motor impairment tested by measuring stride length and base width (distance between foot prints in cm); n = 10 per genotype.

**Supplementary figure 4. *Epm2aip1*$^{-/-}$ mice do not have Lafora disease (12 months-old).**

(A) Hippocampus from an *Epm2aip1*$^{-/-}$ mouse stained with PASD
(B) Hippocampus from a mouse with LD (malin-deficient) stained with PASD; note abundant polyglucosan bodies (numerous PASD-positive granules in the neuropil around asterisks).
(C) Muscle cross section from an *Epm2aip1*$^{-/-}$ mouse stained with PAS-D
(D) Muscle from a mouse with LD (laforin-deficient) stained with PAS-D. Note abundant polyglucosan bodies.

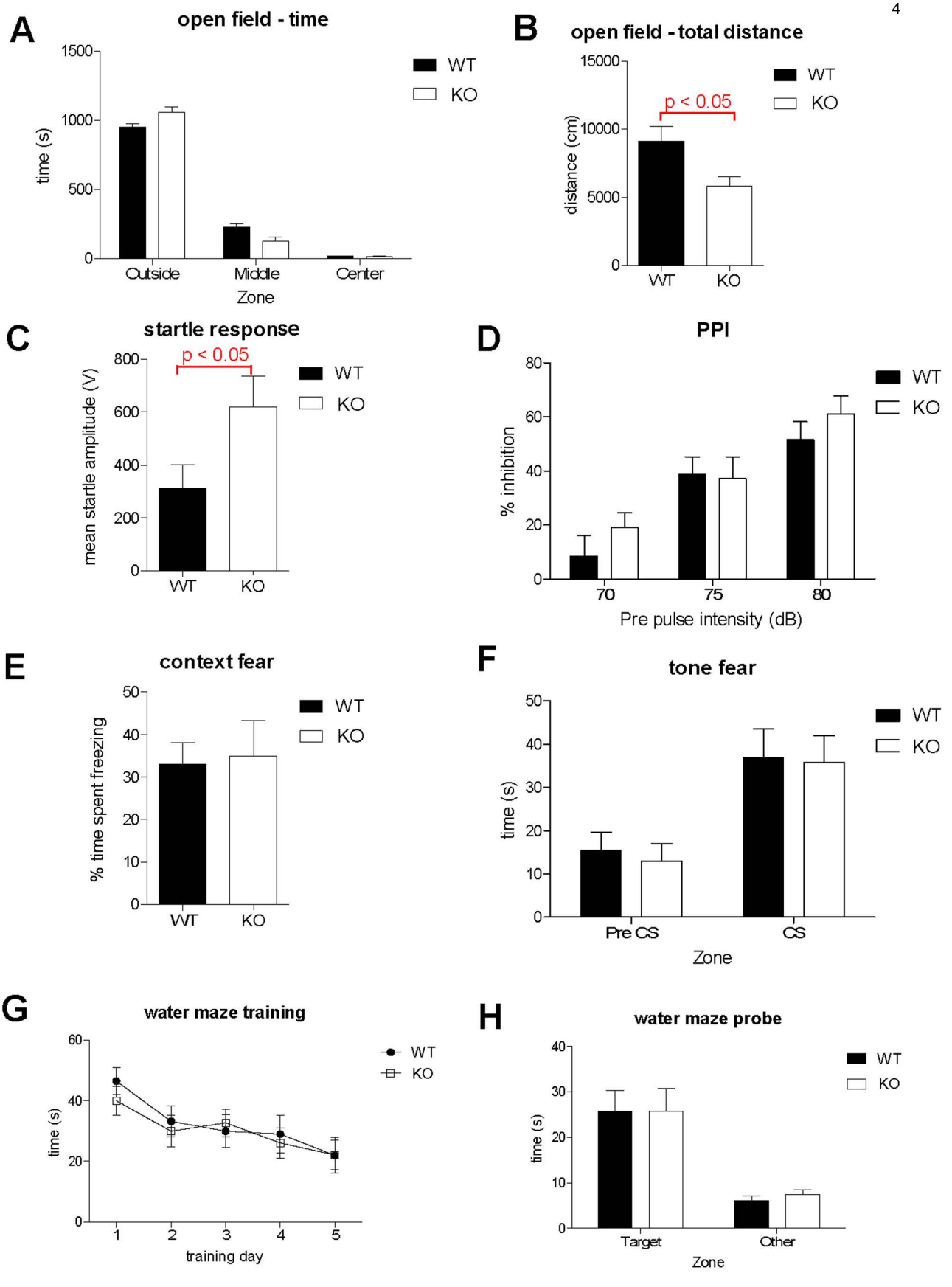
A
open field - time
time (s)
1500
1000
500
0
Outside
Middle
Center
Zone
WT
KO
B
open field - total distance
distance (cm)
15000
10000
5000
0
p < 0.05
WT
KO
C
startle response
mean startle amplitude (V)
800
600
400
200
0
p < 0.05
WT
KO
D
PPI
% inhibition
80
60
40
20
0
70
75
80
Pre pulse intensity (dB)
WT
KO
E
context fear
% time spent freezing
50
40
30
20
10
0
WT
KO
F
tone fear
time (s)
50
40
30
20
10
0
Pre CS
CS
Zone
WT
KO
G
water maze training
time (s)
60
40
20
0
1
2
3
4
5
training day
WT
KO
H
water maze probe
time (s)
40
30
20
10
0
Target
Other
Zone
WT
KO

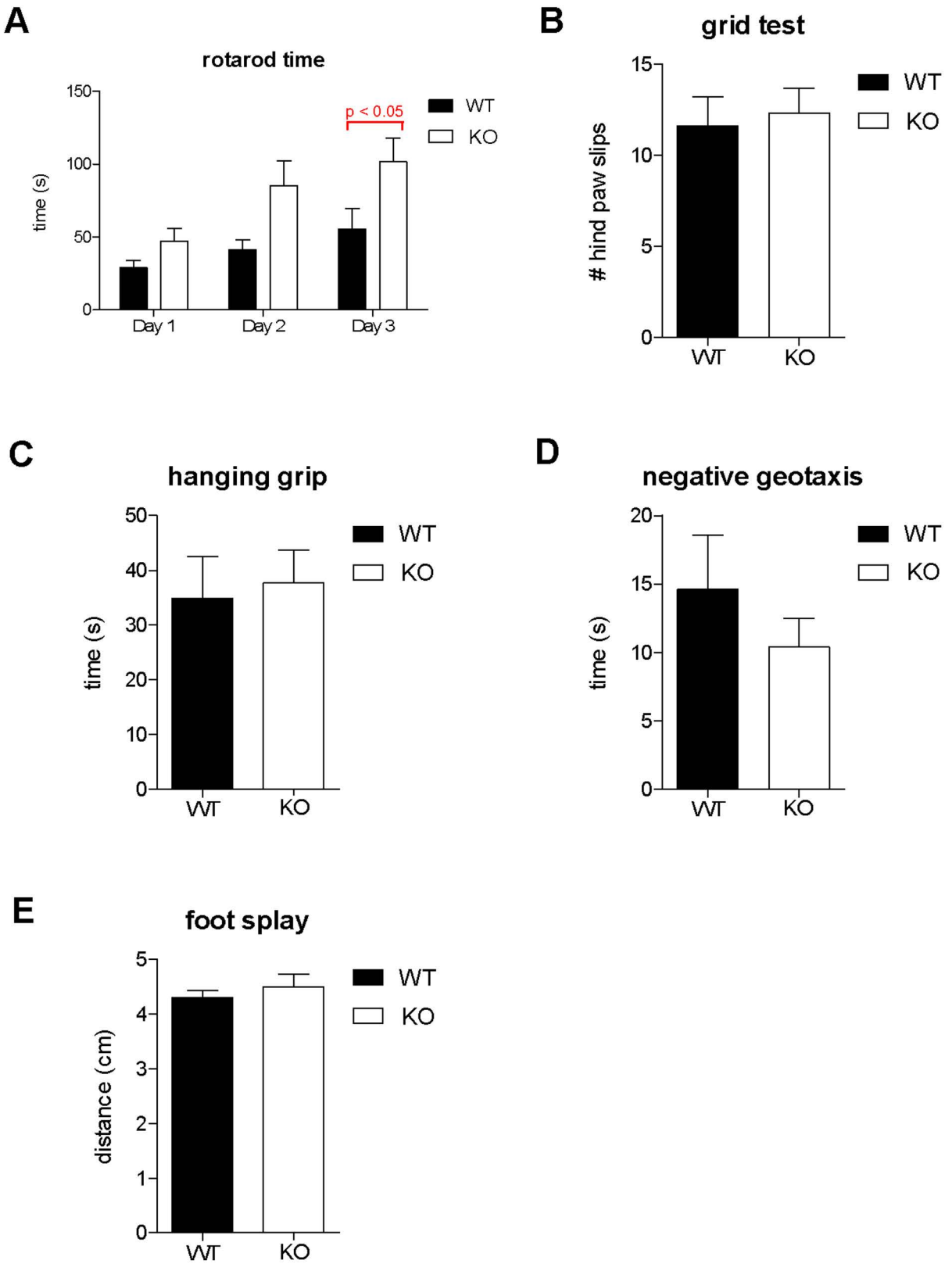
A
rotarod time
time (s)
150
100
50
0
Day 1
Day 2
Day 3
p < 0.05
WT
KO
B
grid test
# hind paw slips
15
10
5
0
WT
KO
C
hanging grip
time (s)
50
40
30
20
10
0
WT
KO
D
negative geotaxis
time (s)
20
15
10
5
0
WT
KO
E
foot splay
distance (cm)
5
4
3
2
1
0
WT
KO

A

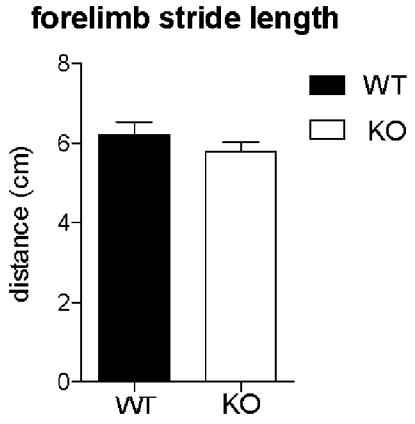
forelimb stride length
distance (cm)
8
6
4
2
0
WT
KO
WT
KO

B

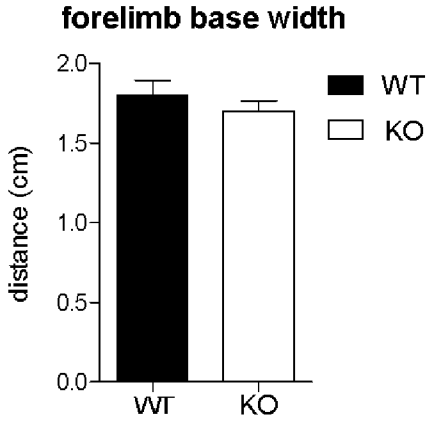
forelimb base width
distance (cm)
2.0
1.5
1.0
0.5
0.0
WT
KO
WT
KO

C

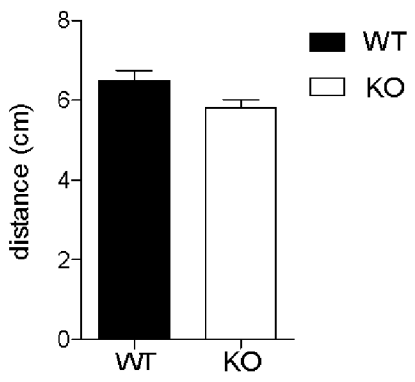
hindlimb stride length
distance (cm)
8
6
4
2
0
WT
KO
WT
KO

D

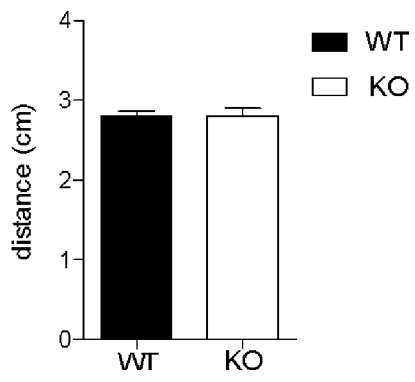
hindlimb base width
distance (cm)
4
3
2
1
0
WT
KO
WT
KO

Figure S4

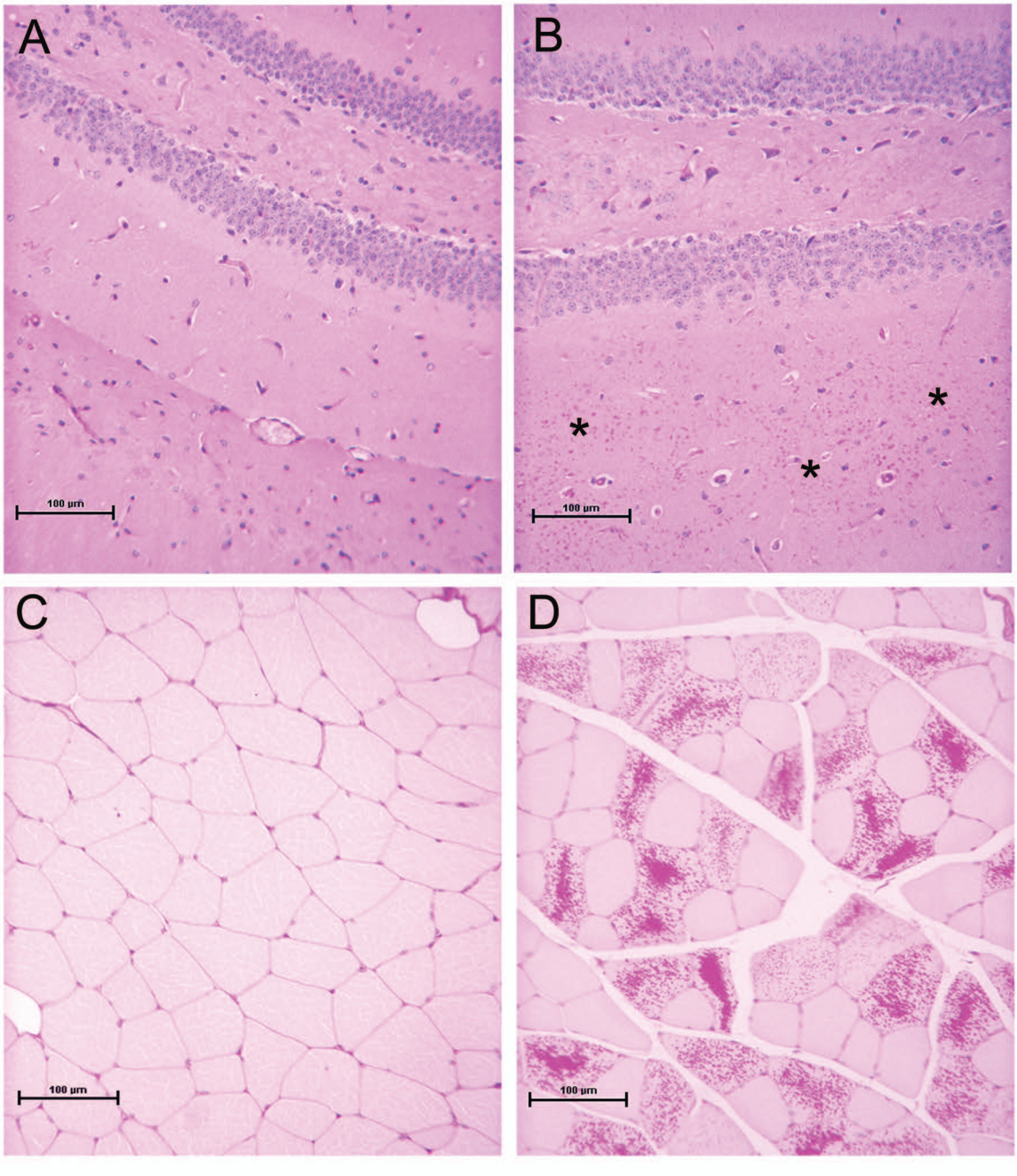

jbc The Journal of Biological Chemistry
AFFINITY SITES
ASBMB American Society for Biochemistry and Molecular Biology

Metabolism:

# Deficiency of a Glycogen Synthase-associated Protein, Epm2aip1, Causes Decreased Glycogen Synthesis and Hepatic Insulin Resistance

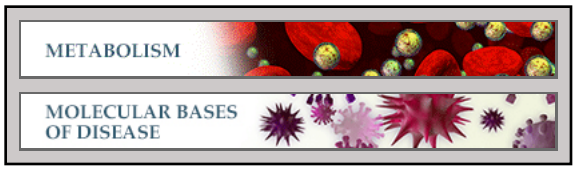


Julie Turnbull, Erica Tiberia, Sandra Pereira, Xiaochu Zhao, Nela Pencea, Anne L. Wheeler, Wen Qin Yu, Alexander Ivovic, Taline Naranian, Nyrie Israelian, Arman Draginov, Mark Piliguian, Paul W. Frankland, Peixiang Wang, Cameron A. Ackerley, Adria Giacca and Berge A. Minassian

*J. Biol. Chem. 2013, 288:34627-34637.*
*doi: 10.1074/jbc.M113.483198 originally published online October 18, 2013*

Access the most updated version of this article at doi: 10.1074/jbc.M113.483198

Find articles, minireviews, Reflections and Classics on similar topics on the JBC Affinity Sites.

Alerts:
- When this article is cited
- When a correction for this article is posted

Click here to choose from all of JBC's e-mail alerts

Supplemental material:
http://www.jbc.org/content/suppl/2013/10/18/M113.483198.DC1.html

This article cites 50 references, 17 of which can be accessed free at
http://www.jbc.org/content/288/48/34627.full.html#ref-list-1

Downloaded from http://www.jbc.org/ by guest on January 1, 2016